

RESEARCH ARTICLE

## Antitumor evaluation and molecular docking study of substituted 2-benzylidenebutane-1,3-dione, 2-hydrazonobutane-1,3-dione and trifluoromethyl-1H-pyrazole analogues

Ibrahim A. Al-Suwaidan<sup>1</sup>, Naglaa I. Abdel-Aziz<sup>2</sup>, Adel S. El-Azab<sup>1,3</sup>, Magda A.-A. El-Sayed<sup>4</sup>, Amer M. Alanazi<sup>1</sup>, Mahmoud B. El-Ashmawy<sup>2</sup>, and Alaa A.-M. Abdel-Aziz<sup>1,2</sup>

<sup>1</sup>Department of Pharmaceutical Chemistry, College of Pharmacy, King Saud University, Riyadh, Saudi Arabia, <sup>2</sup>Department of Medicinal Chemistry, Faculty of Pharmacy, University of Mansoura, Mansoura, Egypt, <sup>3</sup>Department of Organic Chemistry, Faculty of Pharmacy, Al-Azhar University, Cairo, Egypt, and <sup>4</sup>Department of Pharmaceutical Organic Chemistry, Faculty of Pharmacy, University of Mansoura, Mansoura, Egypt

### Abstract

A series of 2-(arylidene)-1-(4-chlorophenyl)-4,4,4-trifluorobutane-1,3-diones (**2–4**), 4-(arylidene)-3-(4-chlorophenyl)-5-(trifluoromethyl)-4H-pyrazoles (**5–7**), 1-(4-chlorophenyl)-4,4,4-trifluoro-2-(2-(aryl)hydrazono)butane-1,3-diones (**8, 9**), 3-(4-chlorophenyl)-4-(2-(aryl)hydrazono)-5-(trifluoromethyl)-4H-pyrazoles (**10, 11**), 2-((3-(4-chlorophenyl)-1-phenyl-5-(trifluoromethyl)-1H-pyrazol-4-yl)methylene)malononitrile (**13**), 2-((5-(4-chlorophenyl)-1-phenyl-3-(trifluoromethyl)-1H-pyrazol-4-yl)methylene)cycloalkan-1-ones (**14, 15**) and 1-(aryl)-3-(5-(4-chlorophenyl)-1-phenyl-3-(trifluoromethyl)-1H-pyrazol-4-yl)prop-2-en-1-ones (**16, 17**) were designed, synthesized and evaluated for their *in vitro* antitumor activity. 1-(4-Chlorophenyl)-4,4,4-trifluoro-2-(2-(4-methoxyphenyl)hydrazono)butane-1,3-dione (**8**) showed potential and broad spectrum antitumor activity compared to the known drug 5-FU with GI<sub>50</sub>, (6.61 and 22.60 μM), TGI (42.66 and <100 μM) and LC<sub>50</sub> (93.33 and <100 μM) values, respectively. On the other hand, compound **8** yielded selective activities toward melanoma, colon, non-small lung and breast cancer cell lines compared with erlotinib and gefitinib. Molecular docking methodology was performed for compound **8** into binding site of B-RAFV600E and EGFR kinases which showed similar binding mode to vemurafenib (PLX4032) and erlotinib, respectively.

### Keywords

Antitumor activity, chalcones, hydrazones, molecular docking, pyrazoles

### History

Received 11 May 2014  
Revised 29 August 2014  
Accepted 29 August 2014  
Published online 28 November 2014

### Introduction

Cancer is a disease characterized by a shift in the controlled mechanisms that govern cell proliferation and differentiation. It is considered as a major health problem worldwide to treat and is the leading cause of human mortality exceeded only by cardiovascular diseases<sup>1–6</sup>. It may require treatment with compounds that could target multiple intracellular components<sup>1–6</sup>. Many of chemotherapeutic agents currently used in cancer therapy are agents which inhibit tumor growth by inhibiting the replication and transcription of DNA. On the other hand, the epidermal growth factor receptor (EGFR) is a cellular trans-membrane tyrosine kinase that is over-expressed in a significant number of human tumors (e.g. breast, ovarian, colon, renal and prostate)<sup>7–13</sup>. Over-expression of EGFR family receptors has always been observed in these tumors, approximately in 60% of all tumors.

A number of small molecule EGFR kinase inhibitors have been evaluated in cancer clinical trials<sup>7–13</sup>, such as gefitinib and erlotinib<sup>7–13</sup>. Moreover, B-RAF mutations are found in all melanoma subtypes but are most common in melanomas derived from skin without chronic sun-induced damage. Melanoma is the most aggressive type of skin cancer in which B-RAFV600E kinase is over-expressed in 63% of all malignant melanomas<sup>14–18</sup>. Vemurafenib (PLX4032) is a drug which targets inhibition of B-RAFV600E kinase<sup>14–18</sup>. It was approved by the U.S. Food and Drug Administration (FDA) for treatment of late-stage melanoma, so inhibition of B-RAFV600E kinase is a very potential avenue for the treatment of melanoma<sup>14–18</sup>.

On the other hand, several heterocyclic compounds are intensively studied to enhance the range of anticancer agents<sup>17–24</sup>. During the last decade, lots of pyrazole anticancer agents were discovered, and such pyrazole core has increasingly attracted the attention of synthetic medicinal chemists<sup>17,18,20–24</sup>. Some small chemical molecules containing pyrazole ring system have been exhibited potent anticancer activities and identified as selective inhibitors of both B-RAFV600E and EGFR kinases<sup>17,18,24</sup>. Moreover, chalcones and hydrazones are an important class of molecules and speculated as promising candidates as anticancer agents<sup>25,26</sup>.

Address for correspondence: Alaa A.-M. Abdel-Aziz, Department of Pharmaceutical Chemistry, College of Pharmacy, King Saud University, Riyadh 11451, Saudi Arabia. Tel: +966-53-5991127. E-mail: alaa\_moenes@yahoo.com

Following these findings, as part of our efforts to design novel antitumor agents, we thus initiated a screening program to search for novel utility of a group of chalcone, hydrazone and pyrazole derivatives as potential antitumor. Moreover, molecular docking methodology was used to identify the structural features required for the antitumor properties of these series. These models are necessary to obtain a consistent and more precise picture of the biological active molecules at the atomic level which can be used to design novel therapeutic agents<sup>27-30</sup>. However, the results of this molecular docking could support the postulation that our active compounds may act on the same enzyme target where EGFR and B-RAFV600E inhibitor act confirming the molecular design of the reported class of antitumor agents.

## Experimental

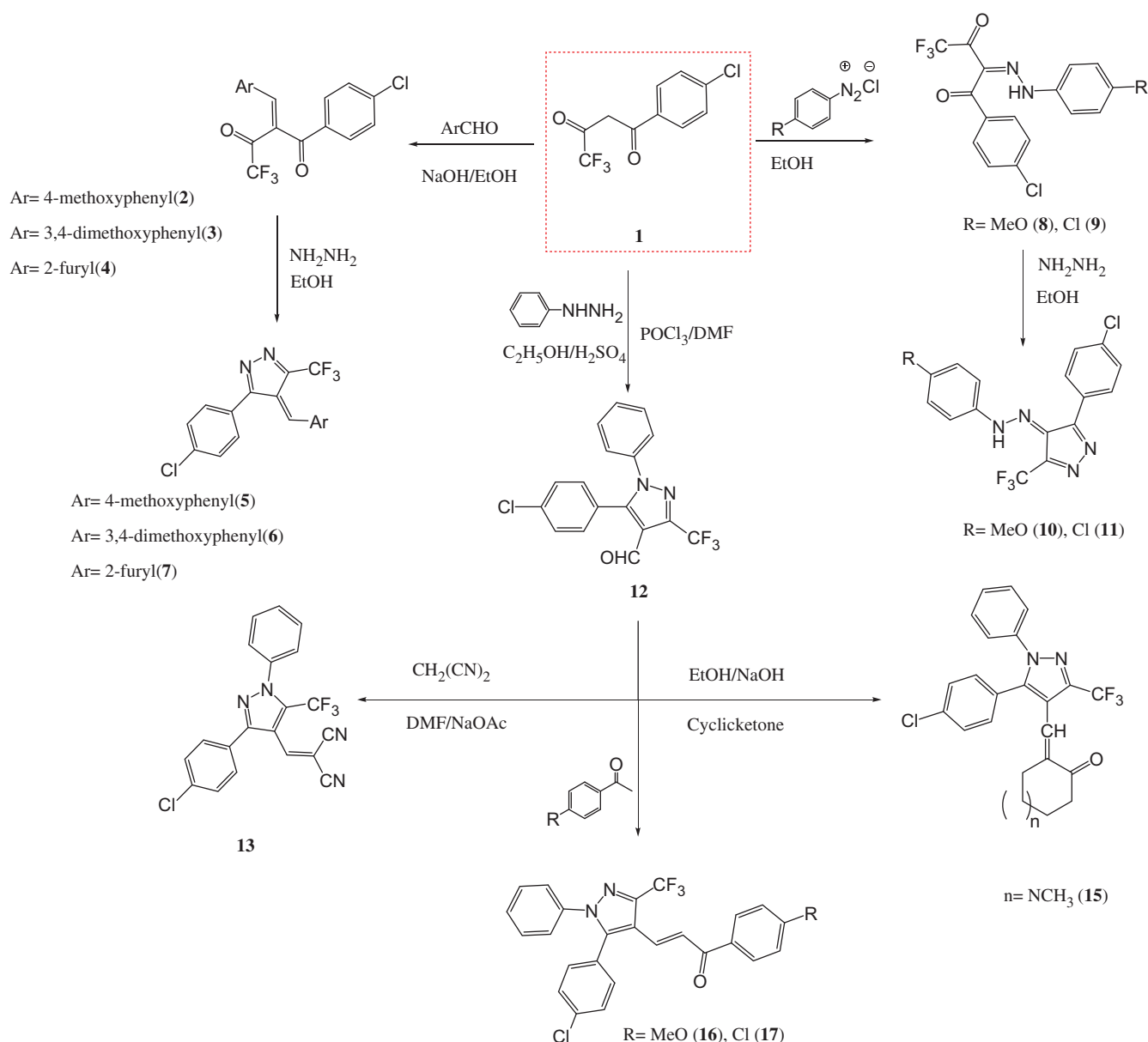
### Synthesis

The target compounds in Scheme 1 were synthesized. The full details of their synthesis, spectroscopic and elemental characterization have been published recently according to our previous reports<sup>28,29</sup>.

## Methodology of the *in vitro* cancer screen

### Full *in vitro* five-dose antitumor assay

A primary anticancer assay was performed for an approximately 60 human tumor cell line panel derived from nine neoplastic diseases, in accordance with the protocol of the Drug Evaluation Branch, National Cancer Institute, Bethesda, MD<sup>31,32</sup>. Tested compounds were added to the culture at a single concentration ( $10^{-5}$  M), and the cultures were incubated for 48 h. End point determinations were made with a protein binding dye, sulforhodamine B (SRB). The results for each tested compound were reported as the growth percentage of the treated cells when compared to that of the untreated control cells. The percentage growth was evaluated spectrophotometrically versus controls not treated with test agents. The cytotoxic and/or growth inhibitory effects of the most active selected compounds were tested *in vitro* against the full panel of about 60 human tumor cell lines at 10-fold dilutions of five concentrations ranging from  $10^{-4}$  to  $10^{-8}$  M. A 48-h continuous drug exposure protocol was followed, and an SRB protein assay was used to estimate cell viability or growth. By use of the seven absorbance measurements [time zero, ( $T_z$ ),



Scheme 1. Synthesis of the designed chalcone, hydrazone and pyrazole analogues.

control growth in the absence of drug ( $C$ ) and test growth in the presence of drug at the five concentration levels ( $T_i$ ), the percentage growth was calculated at each of the drug concentrations levels. Percentage growth inhibition was calculated as:

$$[(T_i - T_z)/(C - T_z) \times 100] \text{ for concentration of which } T_i \geq T_z \quad (1)$$

$$[(T_i - T_z)/T_z] \times 100 \text{ for concentration of which } T_i < T_z. \quad (2)$$

Three dose–response parameters ( $GI_{50}$ , TGI and  $LC_{50}$ ) were calculated for each compound. Growth inhibition of 50% ( $GI_{50}$ ) was calculated from  $[(T_i - T_z)/(C - T_z)] \times 100 = 50$ , which was the drug concentration resulting in a 50% lower net protein increase in the treated cells (measured by SRB staining) compared to the net protein increase seen in the control cells. The drug concentration resulting in total growth inhibition (TGI) was calculated from  $T_i = T_z$ . The  $LC_{50}$  (concentration of drug resulting in a 50% reduction in the measured protein at the end of the drug treatment compared to that at the beginning) indicating a net loss of cells following treatment was calculated from  $[(T_i - T_z)/T_z] \times 100 = -50$ . Values were calculated for each of these three parameters if the level of activity was reached; however, if the effect was not reached or was exceeded, the value for that parameter was expressed as more or less for the maximum or minimum concentration tested. The lowest values are obtained with the most sensitive cell lines. The compounds having  $GI_{50} \leq 100 \mu\text{M}$  were declared to be active.

### Docking methodology

Molecular modeling studies were performed<sup>33</sup> with MOE 2008.10, software available from Chemical Computing Group Inc., 1010 Sherbrooke Street West, Suite 910, Montreal, QC.

#### Selection of protein crystal structures

Ligand-bound crystallographic structures of EGFR and B-RAFV600E kinases are available in the Protein Data Bank<sup>34,35</sup>. In this study, EGFR kinase crystal structure 1M17 and B-RAFV600E kinase were evaluated and selected for docking<sup>34,35</sup>. The errors of the protein were corrected by the structure preparation process in MOE. The first step in the generation of suitable protein structures is the assignment of hydrogen positions on the basis of default rules. Water molecules contained in the PDB file have been removed. Finally, partial charges (the Gasteiger methodology) were calculated, and the active site of the ensemble has been defined as the collection of residues within 10.0 Å of the bound inhibitor and comprised the union of all ligands of the ensemble. All atoms located less than 10.0 Å from any ligand atom were considered.

#### Preparation of the ligand

The ligand coordinates were built using the builder tool of the MOE program<sup>33</sup>. Next, the correct atom types (including hybridization states) and correct bond types were defined, hydrogen atoms were added, charges were assigned to each atom, and finally the structures were energy minimized (MMFF94x, gradient: 0.01)<sup>36</sup>. The energies of ligand structures were previously minimized using the semiempirical AM1 method<sup>37</sup> with MOE program<sup>33</sup>.

#### Docking experiment

The docking experiment on EGFR and B-RAFV600E kinase was carried out by superimposing the energy minimized ligand on

erlotinib in the PDB file 1M17 and vemurafenib in the PDB file 3OG7, respectively, after which erlotinib and vemurafenib were deleted. The default Triangle Matcher placement method was used for docking. GBVI/WSA dG scoring function which estimates the free energy of binding of the ligand from a given pose was used to rank the final poses. The ligand–enzyme complex with lowest  $S\_score$  was selected.

## Results and discussion

### Chemistry

The target compounds in Scheme 1 were synthesized in our laboratories and showed significant anti-inflammatory with COX-2 inhibitory activities. The full details of their synthesis, spectroscopic and elemental characterization were published recently<sup>28,29</sup>.

### Antitumor activity

Twelve compounds **2–7**, **8**, **10** and **13–16** were selected by National Cancer Institute, Bethesda, MD (Tables 1 and 2) on the basis of degree of the structure variation and computer modeling techniques for evaluation of their antitumor activity<sup>31,32</sup>. The selected compounds were subjected to *in vitro* anticancer assay against tumor cells in a full panel of 60-cell lines taken from nine different organs (lung, colon, breast, ovary, blood, kidney, skin, prostate and brain). The compounds **2–7**, **8**, **10** and **13–16** were evaluated at a single dose concentration of 10  $\mu\text{M}$ , the percentages of growth inhibitions over the 60 tested cell lines were determined and the results were compared with 5-fluorouracil as reference drug (Tables 1 and 2). In the screening methodology, each cell line was inoculated and incubated for 24–48 h on a microtiter plate. Test molecules were then added at a single concentration, and the culture was incubated for further 48 h. The end point determinations were made with a protein binding dye, sulforhodamine (SRB). The results for each evaluated molecule were reported as the percentage growth of the treated cells comparing to the untreated control cells. The preliminary screening results and percentages of growth inhibition over sensitive cell lines are shown in Tables 1 and 2.

The synthesized compounds **2–7**, **8**, **10** and **13–16** (Tables 1 and 2) displayed significant activity in the *in vitro* screening on the tested cell lines in 10  $\mu\text{M}$  concentration with positive cytotoxic effect (PCE) of 3/53–46/53. These molecules showed a cytotoxic effect on the most of the cancer cell lines especially compounds **3**, **5**, **7**, **8** and **16** with mean growth inhibition percentages (MGI%) of 15.68, 16.95, 16.79, 37.13 and 9.92%, respectively. Derivatives based on hydrazone **8** were more active compared with the corresponding chalcone **2** and pyrazole **10** analogues as indicated by mean growth inhibition percentages of 37.13, 3.75 and 2.11%, respectively. Moreover, the dimethoxy chalcone **3** (MGI% = 15.68) showed higher antitumor activity than the corresponding mono-methoxy derivative **2** (MGI% = 3.75). Replacement of the 4-methoxybenzylidene with furylidene as in compounds **5** and **7** leads to maintain the antitumor activity with mean growth inhibition percentages of 16.95 and 16.79%, respectively. On the other hand, conversion of compounds **3** and **8** to the corresponding pyrazoles **6** and **10** led to sharp decrease of the antitumor activity with mean growth inhibition percentages of 15.68, 37.13, 0.25, and 2.11%, respectively (Table 1), which may attributed to restricted conformation of compounds **6** and **10** on the receptor binding site. Interestingly, trisubstituted pyrazoles **5** and **7** showed higher activity compared with the tetrasubstituted derivatives **13**, **14**, **15**, and **16** with mean growth inhibition percentages of 16.95, 16.79, 0.81, 2.56, –2.99 and 9.92%, respectively. Moreover, chalcone **16** is more active than the

Table 1. Antitumor activity of chalcone, hydrazone and pyrazole derivatives 2–7, 8, 10 and 13–16 presented as growth inhibition percentages (GI%) over 60 subpanel tumor cell lines.

Compd. No.	60 cell lines assay in one dose 10.0 μM concentration: GI%		
	MGI%	PCE	Most sensitive cell lines
2	3.75	11/59	<i>Leukemia</i> (CCRF-CEM: 10.3%, MOLT-4: 14.2%, SR: 23.8%), <i>NSC Lung Cancer</i> (NCI-H322M: 22.3%, NCI-H522: 25.3%), <i>Colon Cancer</i> (HT29: 17.9%), <i>Melanoma</i> (SK-MEL-2: 13.6%), <i>Renal Cancer</i> (A498: 17.6%, TK-10: 24.7%, UO-31: 21.4%), <i>Breast Cancer</i> (MCF7: 22.9%).
3	15.68	32/59	<i>Leukemia</i> (CCRF-CEM: 34.5%, HL-60(TB): 14.4%, K-562: 53.5%, MOLT-4: 18.8%, PRMI-8226: 70.5%, SR: 70.5%), <i>NSC Lung Cancer</i> (NCI-H226: 13.8%, HOP-92: 18.9%, NCI-H23: 14.4%, NCI-H522: 32.6%), <i>Colon Cancer</i> (COLO 205: 14.9%, HCC-2998: 11.2%, HCT-116: 66.9%, HCT-15: 22.1%, HT29: 36.8%, KM12: 25.6%, SW-620: 47.3%), <i>CNS Cancer</i> (SF-539: 13.3%, SNB-19: 11.6%, U251: 18.7%), <i>Melanoma</i> (LOX IMVI: 32.5%), <i>Ovarian Cancer</i> (OVCAR-3: 10.9%, OVCAR-4: 17.1%, OVCAR-8: 10.6%, NCI/ADR-RES: 10.6%), <i>Renal Cancer</i> (CAKI-1: 13.6%, UO-31: 25.7%), <i>Prostate Cancer</i> (PC-3: 10.2%), <i>Breast Cancer</i> (MCF7: 80.4%, MDA-MB-231/ATCC: 12.1%, T-47D: 25.3%, MDA-MB-468: 16.7%).
4	0.63	8/58	<i>Leukemia</i> (HL-60(TB): 12.5%, MOLT-4: 17.4%, SR: 12.8%), <i>CNS Cancer</i> (SF-295: 12.3%, SNB-75: 11.6%), <i>Melanoma</i> (M14: 41.9%) <i>Renal Cancer</i> (UO-31: 35%), <i>Prostate Cancer</i> (PC-3: 10.3%).
5	16.95	33/58	<i>Leukemia</i> (CCRF-CEM: 73.4%, HL-60(TB): 21.7%, K-562: 51.1%, MOLT-4: 29.4%, PRMI-8226: 18.4%, SR: 59.8%), <i>NSC Lung Cancer</i> (EKVX: 28.7%, HOP-62: 10.9%, NCI-H23: 18.5%, NCI-H226: 12.1%, NCI-H522: 27.7%), <i>Colon Cancer</i> (HCT-116: 70.9%, HCT-15: 15.9%, KM12: 32.8%, SW-620: 31.5%), <i>CNS Cancer</i> (SF-539: 13.7%, SNB-19: 10.1%, SNB-75: 20%, U251: 16.4%), <i>Melanoma</i> (LOX IMVI: 28.4%, UACC-62: 12.6%), <i>Ovarian Cancer</i> (IGROV1: 50.7%, OVCAR-3: 16.4%, OVCAR-8: 14%), <i>Renal Cancer</i> (ACAKI-1: 13.7%, SN12C: 11.3%, UO-31: 56%), <i>Prostate Cancer</i> (PC-3: 13.1%), <i>Breast Cancer</i> (MCF7: 81.5%, MDA-MB-231/ATCC: 20.4%, T-47D: 27.5%, HS 578T: 19.9%, MDA-MB-468: 11.2%).
6	−0.25	9/57	<i>Leukemia</i> (MOLT-4: 20.4%, SR: 13.9%), <i>NSC Lung Cancer</i> (EKVX: 14.3%, NCI-H23: 11%, NCI-H522: 20.1%), <i>Colon Cancer</i> (HCT-15: 10.3%), <i>Renal Cancer</i> (UO-31: 21.4%), <i>Breast Cancer</i> (MCF7: 24.1%, MDA-MB-468: 12%).
7	16.79	33/57	<i>Leukemia</i> (CCRF-CEM: 26.6%, HL-60(TB): 23.8%, K-562: 54.4%, MOLT-4: 16.2%, SR: 58.7%), <i>NSC Lung Cancer</i> (A549/ATCC: 14.7%, NCI-H23: 18.2%, NCI-H460: 13.9%, NCI-H522: 31.2%), <i>Colon Cancer</i> (COLO 205: 11.8%, HCC-2998: 32%, HCT-116: 13.4%, HCT-15: 34.8%, HT29: 39.9%, KM12: 58.6%, SW-620: 31.7%), <i>CNS Cancer</i> (SF-268: 21.4%, SF-295: 12.8%, SNB-75: 12.5%, U251: 27.4%), <i>Melanoma</i> (LOX IMVI: 22.3%, M14: 18.8%, SK-MEL-2: 41.8%, SK-MEL-5: 12.9%, UACC-257: 14.9%, UACC-62: 12%), <i>Ovarian Cancer</i> (OVCAR-3: 17.1%, NCI/ADR-RES: 30.8%), <i>Renal Cancer</i> (CAKI-1: 14.2%, UO-31: 22.2%), <i>Breast Cancer</i> (MCF7: 40.5%, MDA-MB-231/ATCC: 22.3%, MDA-MB-468: 59.2%).
8	37.13	46/53	<i>Leukemia</i> (CCRF-CEM: 58.9%), <i>NSC Lung Cancer</i> (A549/ATCC: 48.8%, HOP-92: 34.8%, NCI-H23: 38.9%, NCI-H322M: 20.1%, NCI-H460: 43.15%, NCI-H522: 51.3%), <i>Colon Cancer</i> (HCC-2998: 30.7%, HCT-116: 42.4%, HCT-15: 61.6%, HT29: 50.9%, KM12: 61.9%, SW-620: 56.7%), <i>CNS Cancer</i> (SF-268: 36.9%, SF-295: 88%, SF-539: 34.1%, SNB-19: 16.6%, SNB-75: 14.7%, U251: 66.4%), <i>Melanoma</i> (LOX IMVI: 75.9%, MALME-3M: 14.0%, M14: 65.9%, MDA-MB-435: 85.0%, SK-MEL-2: 42.7%, SK-MEL-28: 16.3%, SK-MEL-5: 18.1%, UACC-257: 23.0%, UACC-62: 85.1%), <i>Ovarian Cancer</i> (IGROV1: 33.8%, OVCAR-3: 35.7%, OVCAR-5: 59.5%, OVCAR-8: 29.9%, NCI/ADR-RES: 75.2%), <i>Renal Cancer</i> (786-0: 28.3%, A498: 26.4%, ACHN: 20.5%, CAKI-1: 45.1%, SN12C: 20.2%, UO-31: 36.9%), <i>Prostate Cancer</i> (PC-3: 49.2%, DU-145: 26.7%), <i>Breast Cancer</i> (MCF7: 34.8%, MDA-MB-231/ATCC: 51.9%, BT-549: 21.7%, T-47D: 29.6%, HS 578T: 29.0%).
10	2.11	8/51	<i>NSC Lung Cancer</i> (NCI-H522: 14%), <i>Colon Cancer</i> (KM12: 16.4%), <i>Melanoma</i> (MDA-MB-435: 41.4%), <i>Renal Cancer</i> (A498: 44%, UO-31: 19.1%), <i>Breast Cancer</i> (MCF7: 15.6%, T-47D: 16.9%, BT-549: 14.4%).
13	0.81	7/58	<i>Leukemia</i> (MOLT-4: 18.3%), <i>CNS Cancer</i> (SNB-75: 13.1%), <i>Melanoma</i> (MALME-3M: 12.9%, SK-MEL-2: 15.2%), <i>Renal Cancer</i> (TK-10: 11.2%, UO-31: 24.2%), <i>Breast Cancer</i> (T-47D: 10.2%).
14	2.56	12/53	<i>Leukemia</i> (CCRF-CEM: 21.1%), <i>NSC Lung Cancer</i> (A549/ATCC: 17.5%, EKVX: 21.7%), <i>Colon Cancer</i> (HCT-116: 13.6%), <i>Melanoma</i> (UACC-62: 13.2%), <i>Renal Cancer</i> (A498: 21.3%, CAKI-1: 16.1%, UO-31: 18.4%), <i>Breast Cancer</i> (MCF7: 13.8%, MDA-MB-231/ATCC: 12.7%, HS 578T: 12.2%, T-47D: 23.6%).
15	−2.99	3/53	<i>Leukemia</i> (CCRF-CEM: 11%), <i>Renal Cancer</i> (A498: 24.2%, UO-31: 10.1%).
16	9.92	27/54	<i>Leukemia</i> (CCRF-CEM: 14.5%), <i>NSC Lung Cancer</i> (A549/ATCC: 18.7%, HOP-92: 34.9%, NCI-H23: 19.2%, NCI-H460: 17.7%, NCI-H522: 21.1%), <i>Colon Cancer</i> (HCT-116: 36.6%, HCT-15: 22.3%, HT29: 10.1%, KM12: 15.2%), <i>CNS Cancer</i> (SNB-75: 13.9%, U251: 13.7%), <i>Melanoma</i> (LOX IMVI: 25%, SK-MEL-2: 11%, SK-MEL-5: 14.7%, UACC-62: 17.5%), <i>Ovarian Cancer</i> (OVCAR-4: 11%, OVCAR-8: 22.2%, SK-OV-3: 17.3%), <i>Renal Cancer</i> (A498: 12.9%, CAKI-1: 10%, RXF 393: 11.6%, SN12C: 11.9%, UO-31: 25.9%), <i>Breast Cancer</i> (MCF7: 38.2%, MDA-MB-231/ATCC: 20.5%, T-47D: 35.2%).

PCE positive cytotoxic effect in the ratio between number of cell lines with percentage growth inhibition <10% and total number of cell lines.  
MGI% mean growth inhibition percentage.

Table 2. Antitumor activity of the most active chalcone, hydrazone and pyrazole **3**, **5**, **7**, **8** and **16** with GI% over the most sensitive tumor cell line.

60 Subpanel tumor cell lines	% Growth inhibition (GI%)*					5-Flu
	3	5	7	8	16	
<b>Leukemia</b>						
CCRF-CEM	34.5	73.4		58.9		57.1
K-562	53.5	51.1	54.4			42.3
PRMI-8226	70.5					41.4
SR	70.5	59.8	58.7			
<b>Non-small cell lung cancer</b>						
A549/ATCC				48.8		34.2
HOP-92				34.8	34.9	50.6
NCI-H23				38.9		39.0
NCI-H460				43.15		
NCI-H522	32.6		31.2	51.3		58.0
<b>Colon cancer</b>						
HCC-2998			32	30.7		>100
HCT-116	66.9	70.9		42.4	36.6	17.8
HCT-15			34.8	61.6		
HT29	36.8		39.9	50.9		
KM12		32.8	58.6	61.9		40.7
SW-620	47.3	31.5	31.7	56.7		50.1
<b>CNS cancer</b>						
SF-268				36.9		59.0
SF-295				88		69.1
SF-539				34.1		>100
U251				66.4		50.3
<b>Melanoma</b>						
LOX IMVI	32.5			75.9		30.4
M14				65.9		Nt
MDA-MB-435				85.0		36.6
SK-MEL-2			41.8	42.7		95.5
UACC-62				85.1		39.7
<b>Ovarian cancer</b>						
IGROV1		50.7		33.8		51.2
OVCAR-3				35.7		47.4
OVCAR-5				59.5		44.3
NCI/ADR-RES			30.8	75.2		47.6
<b>Renal cancer</b>						
CAKI-1				45.1		39.4
UO-31		56		36.9		41.3
<b>Prostate cancer</b>						
PC-3				49.2		58.2
<b>Breast cancer</b>						
MCF7	80.4	81.5	40.5	34.8	38.2	
MDA-MB-231/ATCC				51.9		78.1
T-47D					35.2	56.7
MDA-MB-468			59.2			Nt

5-Flu, 5-fluorouracil; Nt, not tested

\*Only GI % higher than 30% are shown.

corresponding cyclic analogues **14** and **15** with mean growth inhibition percentages of 9.92, 2.56 and -2.99%, respectively.

By investigating the variation in selectivity and broad spectrum of the tested compounds over the full panel of cell lines, it was revealed that nearly five of the tested derivatives (Tables 1 and 2) showed significant inhibition for the most cell lines used in this assay with growth inhibition reached to 88% and are mainly active against leukemia, non-small cell lung (NSCLC), colon, CNS, melanoma, ovarian, renal and breast cell lines with growth inhibition reached to 73.4, 51.3, 70.9, 88.0, 85.1, 75.2, 56, and 81.5%, respectively.

Compounds **3**, **5**, **7**, **8** and **16** showed broad spectrum and significant inhibition for cancer cells (59 cell lines;

Tables 1 and 2) and possessed a considerable cytotoxic activity against cell lines of leukemia (GI% = 34.5–73.4), non-small cell lung (GI% = 31.2–51.3), colon (GI% = 30.7–70.9), CNS (GI% = 34.1–88.0), melanoma (GI% = -32.5–85.1), ovarian (GI% = 30.8–75.2), renal (GI% = 36.9–56) and breast (GI% = 34.8–81.5). This great inhibition at the mentioned concentration indicates a great potency for the compounds **3**, **5**, **7**, **8** and **16** with a strong lethal effect over cancer cells.

Regarding the activity toward individual cell lines (Tables 1 and 2), compounds **3** and **5** showed selective activity against leukemia cell lines CCRF-CEM, K-562, SR and PRMI-8226 with GI% values of 34.5, 53.5, 70.5, 70.5, 73.4, 51.1, 59.8 and 18.4, respectively. Non-small cell lung NCI-H522 cell line proved to be selectively sensitive to **3**, **5**, **7**, **8** and **16** with GI% values of 32.6, 27.7, 31.2, 51.3 and 21.1, respectively. In addition, compounds **8** and **16** proved to have equal susceptibility to the HOP-92 cell line with GI% values of 34.8 and 34.9, respectively. Compound **8** have broad spectrum activity against non-small cell lung A549/ATCC, HOP-92, NCI-H23, NCI-H322M, NCI-H522 and NCI-H460 cell lines with GI% values of 48.8, 34.8, 38.9, 20.1, 51.3 and 43.1, respectively. Concerning colon cancer, compounds **3**, **5**, **7**, **8** and **16** showed GI% values of 25.6, 32.0, 58.6, 61.9, 15.2, 66.9, 70.9, 13.4, 42.4 and 36.8 with colon KM12 and HCT-116 cell lines, respectively. On the other hand, compounds **3**, **5**, **7**, **8** and **16** verified sensitivity in 22.1, 15.9, 34.8, 61.6 and 22.3% to colon HCT-15 cancer cells. Respecting melanoma, compounds **3**, **5**, **7**, **8** and **16** are active against LOX IMVI cell lines with GI% values of 32.5, 28.4, 22.3, 75.9 and 25.0, respectively. Compound **8** showed broad spectrum activities against melanoma LOX IMVI, M14, MDA-MB-435, SK-MEL-28, SK-MEL-2, SK-MEL-5, UACC-257 and UACC-62 cell lines with GI% values of 75.9, 65.9, 85.0, 16.3, 42.7, 18.1, 23.0 and 85.1. Pertaining to renal cancer, compounds **3**, **5**, **7**, **8** and **16** were active against UO-31 cell line with GI% values of 25.7, 56.0, 22.2, 36.9 and 25.9, respectively. Renal CAKI-1 cell line sensitive to compound **8** with GI% value of 45.1. Relating to breast cancer, breast MCF7, MDA-MB-231/ATCC, T-47D and MDA-MB-468 cell lines possess convinced responsive to compounds **3**, **5**, **7**, **8** and **16** with GI% values from 16 to 81%. Compounds **5** and **8** showed GI% effectiveness against breast HS 578T cell line with values of 19.9 and 29.0, respectively. On the other hand, ovarian IGROV1, OVCAR-3, OVCAR-5 and NCI/ADR-RES cell lines receptive to compound **8** with GI% values of 33.8, 35.7, 59.5 and 75.2, respectively. Additionally, compound **5** demonstrated remarkable activities to IGROV1 with GI% value of 50.7, while NCI/ADR-RES cell line sensitive to compound **7** with GI% value 30.8.

Finally, compound **8** was selected in advanced assay against a panel of approximately 60 tumor cell lines at 10-fold dilution of five concentrations (100, 10, 1, 0.1 and 0.01  $\mu$ M), and the results were compared with 5-fluorouracil, gefitinib and erlotinib as reference drugs (Tables 3 and 4; Figure 1). Based on the cytotoxicity assays, three antitumor activity dose-response parameters were calculated for experimental molecule against each cell lines: GI<sub>50</sub>, molar concentration of the compound that inhibits 50% net cell growth; TGI, molar concentration of the compound leading to total inhibition; LC<sub>50</sub>, molar concentration of the compounds leading to 50% net cell death (Tables 3 and 4; Figure 1). Furthermore, mean graph midpoints (MG\_MID) were calculated for each of the parameters, giving an average activity parameter over all cell lines for the tested molecules (Tables 3 and 4; Figure 1).

The above screening data analysis indicated that compound **8** (Tables 3 and 4; Figure 1) possessed potent *in vitro* antitumor activity, with mean GI<sub>50</sub> values across the 60 cell lines ranging from 1.84 to 11.00  $\mu$ M. Mean GI<sub>50</sub>, TGI and LC<sub>50</sub> of compound **8** in comparison with standard anticancer agent 5-fluorouracil

Table 3. Compounds **8** and **5-Flu** median growth inhibitory (GI<sub>50</sub>, μM), total growth inhibitory (TGI, μM) and median lethal (LC<sub>50</sub>, μM) concentration of *in-vitro* subpanel tumor cell lines.

Compd.	Activity	Subpanel tumor cell lines									
		Leukemia	NSC lung cancer	Colon cancer	CNS cancer	Melanoma	Ovarian cancer	Renal cancer	Prostate cancer	Breast cancer	MG-MID*
<b>8</b>	GI <sub>50</sub>	5.08	9.90	5.46	8.73	5.20	11.40	10.43	12.5	6.55	6.61
	TGI	60.73	37.09	46.20	52.85	43.33	66.31	60.86	85.45	49.75	42.66
	LC <sub>50</sub>	>100	85.91	84.4	>100	93.69	98.1	94.04	>100	>100	93.33
<b>5-FU</b>	GI <sub>50</sub>	15.1	>100	8.4	72.1	70.6	61.4	45.6	22.7	76.4	22.60
	TGI	>100	>100	>100	>100	>100	>100	>100	>100	>100	>100
	LC <sub>50</sub>	>100	>100	>100	>100	>100	>100	>100	>100	>100	>100

\*Full panel mean-graph midpoint (μM).

Table 4. GI<sub>50</sub> values (μM) of compound **8**, gefitinib and erlotinib over the most sensitive cell lines of non-small lung cancer, colon cancer, melanoma, breast cancer, CNS cancer and leukemia subpanels.

Subpanel tumor cell lines	GI <sub>50</sub> (μM)		
	<b>8</b>	Gefitinib	Erlotinib
Non-small cell lung cancer			
A549/ATCC	3.83	7.9	7.9
NCI-H460	3.77	6.3	5.0
NCI-H23	11.0	15.9	20.0
NCI-H522	4.93	6.3	1.0
Colon cancer			
KM12	2.61	7.9	63.1
HT29	4.60	4.0	50.1
HCC-2998	4.01	10.0	79.4
HCT-15	4.68	5.0	3.2
SW-620	4.36	7.9	50.1
Ovarian cancer			
IGROV1	3.69	0.20	0.25
OVCAR-4	4.54	7.94	19.95
OVCAR-8	4.58	10.0	7.94
NCI/ADR-RES	8.87	12.59	6.31
SK-OV-3	2.89	0.63	0.40
Melanoma			
LOX IMVI	3.29	7.9	5.0
M14	2.84	5.0	6.3
MDA-MB-435	2.49	3.2	15.9
SK-MEL-2	2.78	12.6	12.6
SK-MEL-5	3.63	4.0	15.8
Breast cancer			
MCF7	4.11	10	100
T-47D	5.98	6.3	3.2
MDA-MB-468	1.84	0.01	0.2
CNS cancer			
SF-295	2.67	2.0	15.9
SF-539	6.33	10	12.6
U251	4.55	10	20.0
Leukemia			
CCRF-CEM	4.61	5.0	15.9
K-562	3.47	2.5	15.9
SR	4.26	3.2	6.3

(5-Flu) are given in Table 3. This compound **8** ranks as nearly 3-fold more potent compared with the reference standard 5-Flu as indicated by mean GI<sub>50</sub> of 6.61 and 22.6 μM, respectively.

Moreover, comparison of the antitumor activity presented as GI<sub>50</sub> (μM) values of compound **8** with the activity of gefitinib and erlotinib was performed against non-small lung cancer (A549/ATCC, NCI-H460, NCI-H23 and NCI-H522), colon cancer (KM12, HT29, HCC-2998, HCT-15 and SW-620), breast cancer (MCF7, T-47D and MDA-MB-468) cell lines in which EGFR was over-expressed (Table 4; Figure 1). In addition, melanoma

(LOX IMVI, M14, MDA-MB-435, SK-MEL-2 and SK-MEL-5) cell line expresses high levels of B-RAFV600E kinase (Tables 3 and 4; Figure 1). Results indicated that compound **8** is more active than gefitinib and erlotinib against most selected cell lines except non-small lung (NCI-H522) and breast cancer (MDA-MB-468) cell lines. Moreover, compound **8** is more potent than gefitinib and erlotinib against all selected melanoma cell lines and showed the lowest GI<sub>50</sub> values.

The SAR study revealed that (1) potent antitumor activity of tested compounds depended on the presence of a hydrazone and chalcone scaffolds which were more active in comparison with pyrazole analogue; (2) attachment of trisubstituent to pyrazole ring system increases the activity in comparison with tetrasubstituted pyrazole; (3) introduction of two methoxy groups at the chalcone part led to the enhancement of activity; (4) one methoxy group favors the activity of pyrazole core, while two methoxy moieties favor the activity of chalcone core. This would indicate that increase of electron density on chalcone moiety is important for the inhibitory activity; (5) replacement of the arylidene attached to pyrazole with steric bulky chalcone fragment led to decrease of the antitumor activity.

#### Molecular modeling and computational studies

The level of antitumor activities of the compound **8** over breast cancer, colon, renal, small lung and melanoma cancer cells, in which epidermal growth factor receptor (EGFR) and B-RAFV600E kinases are highly expressed, prompted us to perform molecular docking into the ATP binding site of EGFR and B-RAFV600E kinase to predict if this compound has analogous binding mode to the EGFR and B-RAFV600E kinase inhibitors. We assumed that the active target compound **8** might demonstrate antiproliferative activity against breast cancer, colon, renal, small lung and melanoma cell lines through inhibition of EGFR and B-RAFV600E.

Compound **8** was docked into receptor active site of EGFR along with their inhibitor (Figure 2). All calculations were performed using MOE 2008.10 software<sup>33</sup> installed on 2.4G Core (TM) i7. The crystal structure of epidermal growth factor receptor with erlotinib (*Tarceva*<sup>TM</sup>) (PDB code: 1M17)<sup>34</sup> was obtained from protein data bank (PDB). The automated docking program of MOE 2008.10 was used to dock compound **8** along with the inhibitor erlotinib into ATP binding site of EGFR. The complexes were energy-minimized with a MMFF94 force field<sup>36</sup> till the gradient convergence 0.01 kcal/mol was reached. The binding energies of compound **8** and erlotinib docked into the active site of EGFR were −24.99 and −27.03 kcal/mol, respectively (Figure 2). These docking studies have revealed that a water (HOH-10) molecule-mediated hydrogen bonding interaction is observed between the methoxy group of 4-methoxyphenyl fragment and the Thr-766 side chain. This interaction revealed

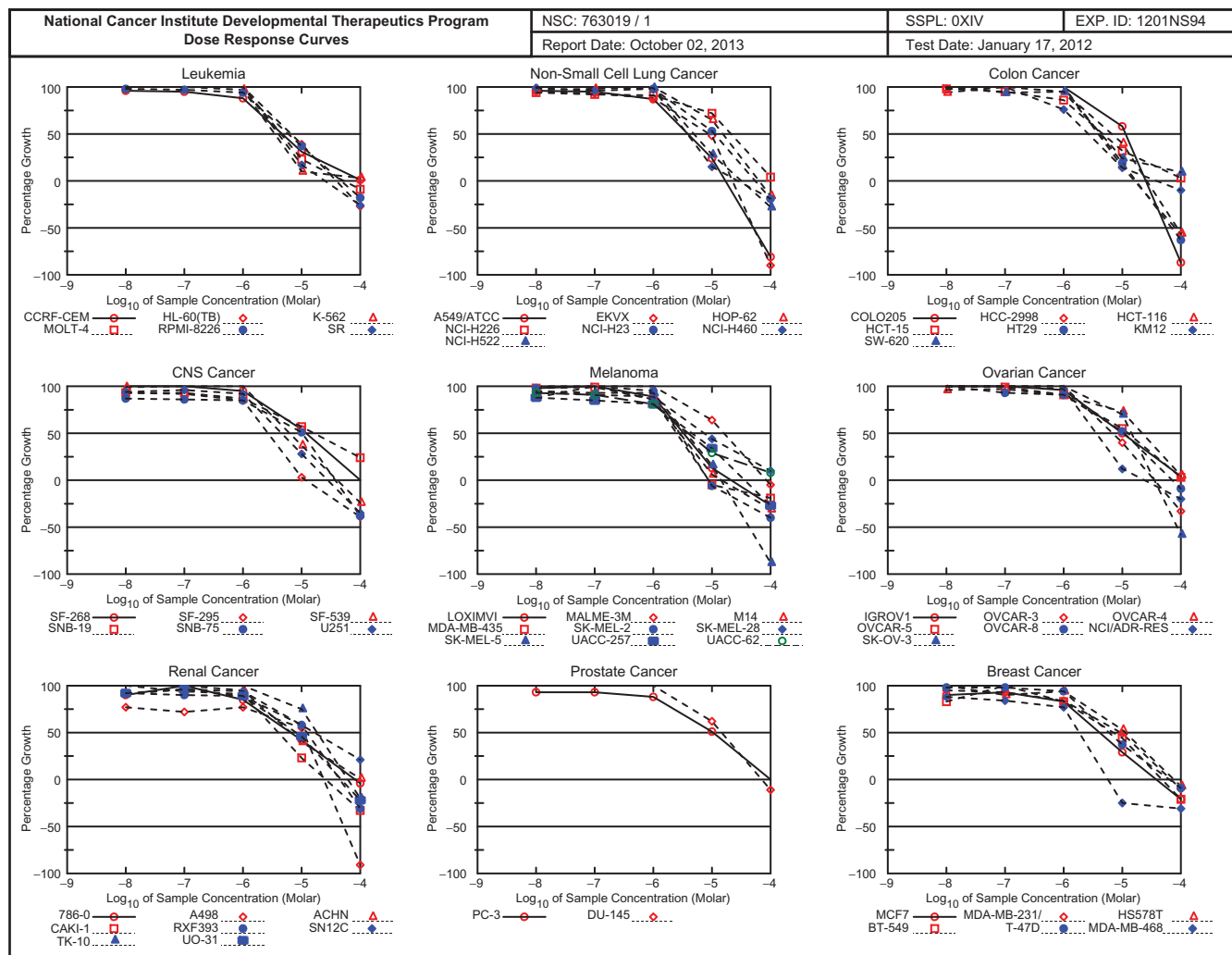


Figure 1. Dose-response curves (% growth versus sample concentration at NCI fixed protocol,  $\mu\text{M}$ ) obtained from the NCI's *in-vitro* disease-oriented human tumor cells line of compound **8** on nine cancer disease.

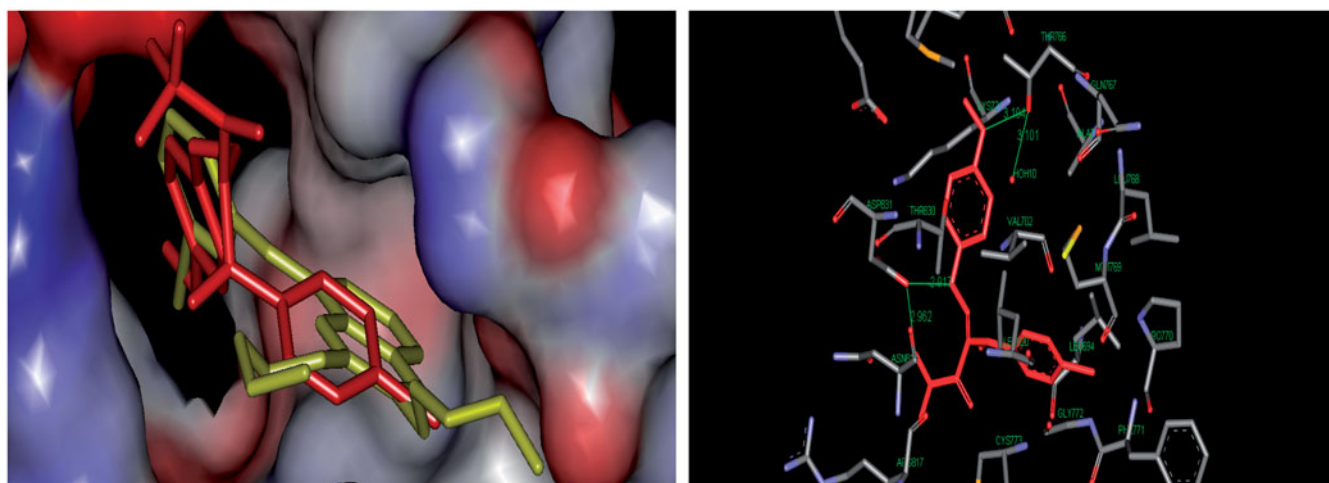


Figure 2. Right panel shows docking studies on compound **8** with active site of epidermal growth factor receptor and left panel shows superimposition of compound **8** (red colored) on erlotinib (yellow colored) inside the pockets of active site. Hydrogen bonds are shown in green.

the importance of 4-methoxyphenyl fragment for binding and the subsequent inhibitory capacity. Similarly, the NH atom of hydrazone part and trifluoromethyl fragment interact with the amino acid Asp-831. Compound **8** complexed with EGFR-TK in a

fashion similar to erlotinib and showed the occurrence of three hydrogen bonds with and HOH-10 (3.19 Å)-mediated hydrogen bonding interaction with Thr-766 side chain. Moreover, the hydrazone NH atom and CF<sub>3</sub> fragment showed two additional

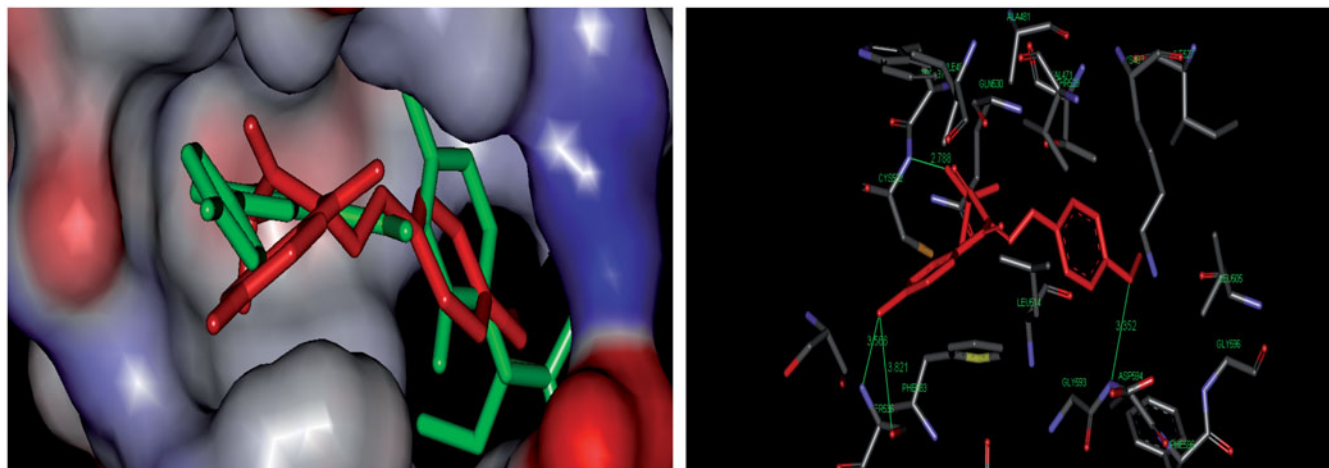


Figure 3. *Right panel* shows docking studies on compound **8** with B-RAFV600E kinase domain and *left panel* shows superimposition of compound **8** (red colored) on PLX4032 inhibitor (green colored) inside the pockets of active site. Hydrogen bonds are shown in green.

hydrogen bonds with Asp-831 (2.91 and 2.96 Å, respectively). In short, Figure 2 demonstrates binding model of hydrazone **8** in the ATP binding site, and the results of this molecular docking could support the postulation that our active compound may act on the same enzyme target where EGFR inhibitor acts confirming the molecular design of the reported class of antitumor agents<sup>11,12,18,24</sup>.

On the other hand, the level of antitumor activities of the compound **8** over melanoma cancer cells, in which B-RAFV600E kinase is highly expressed<sup>14–17,35</sup>, prompted us to perform molecular docking into the ATP binding site of B-RAFV600E kinase to predict if this compound **8** has analogous binding mode to the V600E-B-RAF kinase inhibitors (Figure 3). The crystal structure of B-RAFV600E kinase in complex with vemurafenib (PLX4032, PDB code: 3OG7) was obtained from protein data bank (PDB)<sup>35</sup>. The binding energies of compound **8** and vemurafenib docked into the active site of B-RAFV600E kinase were  $-33.01$  and  $-37.77$  kcal/mol, respectively (Figure 3). The docking study has revealed that the ligand **8** has bound in the active site of one of the protomers in the protein dimer through the formation of four hydrogen bonds (classical and non-classical) with Asp-549 (3.35 Å), Cys-532 (2.78 Å) and Ser-536 (3.56 and 3.82 Å). Moreover, there was one arene  $\pi$ – $\pi$  between the binding site and the ligand **8** which occurred between 4-chlororpenyl fragment and Phe-583. The results of this molecular docking study can support the postulation that our active compound may inhibit the growth of melanoma cell lines through inhibition of B-RAF kinase, similar to vemurafenib<sup>16,18</sup>.

## Conclusion

Twelve different compounds based on hydrazone, chalcone and their pyrazole analogues were evaluated for their antitumor activity, where most of the tested compounds exhibited significant antitumor activity. Amongst the compounds tested, **3**, **5**, **7**, **8** and **16** were found to be most potent. From the detailed analysis of the results of above studies, we conclude that antitumor activity of the synthesized compounds significantly depends on the conformation flexibility of the opened structure and this activity decreased by restricted conformation of pyrazole ring. Molecular docking studies further supported the potent antitumor activity of **8** compared with EGFR and B-RAFV600E kinase inhibitors and further help understanding the various interactions between the ligands and enzyme active sites in detail and thereby help to design novel potent derivatives.

## Declaration of interest

The authors would like to extend their sincere appreciation to the Deanship of Scientific Research at King Saud University for funding this research group No. (RG-1435-046).

## References

1. Myers CE, Chabner BA. Anthracyclines. In: Chabner BA, Collins JM, eds. Cancer chemotherapy: principles and practice. Philadelphia (PA): Lippincott; 1990:314–28.
2. Varmus H. The new era in cancer research. *Science* 2006;312:1162–5.
3. Tsai JY, Lee MJ, Chang MD, et al. Effects of novel human cathepsin S inhibitors on cell migration in human cancer cells. *J Enzyme Inhib Med Chem* 2014;29:538–46.
4. Kucukoglu K, Gul HI, Cetin-Atalay R, et al. Synthesis of new N,N'-bis[1-aryl-3-(piperidine-1-yl)propylidene]hydrazine dihydrochlorides and evaluation of their cytotoxicity against human hepatoma and breast cancer cells. *J Enzyme Inhib Med Chem* 2014; 29:420–6.
5. Sharma A, Tiwari M, Supuran CT. Novel coumarins and benzocoumarins acting as isoform-selective inhibitors against the tumor-associated carbonic anhydrase IX. *J Enzyme Inhib Med Chem* 2014;29:292–6.
6. Eckhardt S. Recent progress in the development of anticancer agents. *Curr Med Chem* 2002;2:419–39.
7. Fricker J. Tyrosine kinase inhibitors: the next generation. *Lancet Oncol* 2006;7:621.
8. Sadek MM, Serrya RA, Kafafy AH, et al. Discovery of new HER2/EGFR dual kinase inhibitors based on the anilinoquinazoline scaffold as potential anti-cancer agents. *J Enzyme Inhib Med Chem* 2014;29:215–22.
9. Srinivasan M, Trivadi SG. Tyrosine kinase inhibitors in cancer therapy. *Clin Biochem* 2004;37:618–35.
10. Bridges AJ. The rationale and strategy used to develop a series of highly potent, irreversible, inhibitors of the epidermal growth factor receptor family of tyrosine kinases. *Curr Med Chem* 1999;6:825–43.
11. Barlesi F, Tchouhadjian C, Doddoli C, et al. Gefitinib (ZD1839, Iressa) in non-small-cell lung cancer: a review of clinical trials from a daily practice perspective. *Fundam Clin Pharmacol* 2005;19:385–93.
12. Ganjoo KN, Wakelee H. Review of erlotinib in the treatment of advanced non-small cell lung cancer. *Biol Targets Ther* 2007;1:335–46.
13. Dhillon S, Wagstaff AJ. Lapatinib. *Drugs* 2007;67:2101–8.
14. Harris PA. Cancer drug design and discovery. 2nd ed. San Diego (CA): Academic Press; 2014:529–63.
15. Brose MS, Volpe P, Feldman M, et al. BRAF and RAS mutations in human lung cancer and melanoma. *Cancer Res* 2002;62:6997–7000.
16. Luo C, Xie P, Marmorstein RJ. Identification of BRAF inhibitors through in silico screening. *Med Chem* 2008;51:6121–7.

17. Kim MH, Kim M, Yu H, et al. Structure based design and syntheses of amino-1H-pyrazole amide derivatives as selective Raf kinase inhibitors in melanoma cells. *Bioorg Med Chem* 2011;19:1915–23.
18. Choi W-K, El-Gamal MI, Choi HS, et al. New diarylureas and diarylamides containing 1,3,4-triarylpyrazole scaffold: synthesis, antiproliferative evaluation against melanoma cell lines, ERK kinase inhibition, and molecular docking studies. *Eur J Med Chem* 2011; 46:5754–62.
19. Yurttaş L, Özkay Y, Akalın-Çiftçi G, et al. Synthesis and anticancer activity evaluation of N-[4-(2-methylthiazol-4-yl)phenyl]acetamide derivatives containing (benz)azole moiety. *J Enzyme Inhib Med Chem* 2014;29:175–84.
20. Manfredini S, Bazzanini R, Baraldi PG, et al. Pyrazole-related nucleosides. 4. Synthesis and antitumor activity of some 1-tetrahydropyran-4-substituted pyrazoles. *Anti-Cancer Drug Des* 1996;11:193–204.
21. Park H-A, Lee K, Park S-J, et al. Identification of antitumor activity of pyrazole oxime ethers. *Bioorg Med Chem Lett* 2005;15: 3307–12.
22. Liu XH, Ruan BF, Liu JX, et al. Design and synthesis of N-phenylacetyl (sulfonyl) 4,5-dihydropyrazole derivatives as potential antitumor agents. *Bioorg Med Chem Lett* 2011;21: 2916–20.
23. Lv PC, Li HQ, Sun J, et al. Synthesis and biological evaluation of pyrazole derivatives containing thiourea skeleton as anticancer agents. *Bioorg Med Chem* 2010;18:4606–14.
24. Lv PC, Li DD, Li QS, et al. Synthesis, molecular docking and evaluation of thiazolyl-pyrazoline derivatives as EGFR TK inhibitors and potential anticancer agents. *Bioorg Med Chem Lett* 2011; 21:5374–7.
25. Go ML, Wu X, Liu XL. Chalcones: an update on cytotoxic and chemoprotective properties. *Curr Med Chem* 2005;12:481–99.
26. Rollas S, Küçükgül SG. Biological activities of hydrazone derivatives. *Molecules* 2007;12:1910–39.
27. Al-Suwaidan IA, Alanazi AM, El-Azab AS, et al. Molecular design, synthesis and biological evaluation of cyclic imides bearing benzenesulfonamide fragment as potential COX-2 inhibitors. Part 2. *Bioorg Med Chem Lett* 2013;23:2601–5.
28. El-Sayed MA-A, Abdel-Aziz NI, Abdel-Aziz AA-M, et al. Design, synthesis, and biological evaluation of substituted hydrazone and pyrazole derivatives as selective COX-2 inhibitors: molecular docking study. *Bioorg Med Chem* 2011;19:3416–24.
29. El-Sayed MA-A, Abdel-Aziz NI, Abdel-Aziz AA-M, et al. Synthesis, biological evaluation and molecular modeling study of pyrazole and pyrazoline derivatives as selective COX-2 inhibitors and anti-inflammatory agents. Part 2. *Bioorg Med Chem* 2012;20: 3306–16.
30. Goda FE, Abdel-Aziz AA-M, Ghoneim HA. Synthesis and biological evaluation of novel 6-nitro-5-substituted aminoquinolines as local anesthetic and anti-arrhythmic agents: molecular modeling study. *Bioorg Med Chem* 2005;13:3175–83.
31. Grever MR, Schepartz SA, Chabner BA. The National Cancer Institute: cancer drug discovery and development program. *Semin Oncol* 1992;19:622–38.
32. Shoemaker RH. The NCI60 human tumour cell line anticancer drug screen. *Nat Rev Cancer* 2006;6:813–23.
33. MOE 2008.10 of Chemical Computing Group. Inc. <http://www.chemcomp.com>.
34. Stamos J, Sliwkowski MX, Eigenbrot C. Structure of the epidermal growth factor receptor kinase domain alone and in complex with a 4-anilinoquinazoline inhibitor. *J Biol Chem* 2002;277:46265–72.
35. Bollag G, Hirth P, Tsai J, et al. Clinical efficacy of a RAF inhibitor needs broad target blockade in BRAF-mutant melanoma. *Nature* 2010;467:596–9.
36. Halgren TA. Merck molecular force field. I. Basis, form, scope, parameterization, and performance of MMFF94. *J Comput Chem* 1996;17:490–519.
37. Dewar MJS, Zebisch EG, Healey EF, et al. Development and use of quantum mechanical molecular models. 76. AM1: a new general purpose quantum mechanical molecular model. *J Am Chem Soc* 1985;107:3902–9.